Classification: BIOLOGICAL SCIENCES, Biochemistry

Quantitative proteomics indicate a strong correlation of mitotic phospho-/dephosphorylation with non-structured regions of substrates

Hiroya Yamazaki[a], Hidetaka Kosako[b], and Shige H. Yoshimura[a, 1]

[a] Graduate School of Biostudies, Kyoto University, Kyoto, Japan, [b] Division of Cell Signaling, Fujii Memorial Institute of Medical Sciences, Tokushima University, Tokushima, Japan.

[1]Corresponding author:

Shige H. Yoshimura

Laboratory of Plasma Membrane and Nuclear Signaling,

Graduate School of Biostudies, Kyoto University,

Yoshida Konoe, Sakyo-ku, Kyoto 606-8501, Japan

Tel & Fax: +81-75-753-7906

E-mail: yoshimura@lif.kyoto-u.ac.jp

Keywords: phosphorylation, mitosis, intrinsically disordered region

Abstract

Protein phosphorylation plays a critical role in the regulation and progression of mitosis. More than 10,000 phosphorylated residues and the associated kinases have been identified to date via proteomic analyses. Although some of these phosphosites are associated with regulation of either protein-protein interactions or the catalytic activity of the substrate protein, the roles of most mitotic phosphosites remain unclear. In this study, we examined structural properties of mitotic phosphosites and neighboring residues to understand the role of heavy phosphorylation in non-structured domains. Quantitative mass spectrometry analysis of mitosis-arrested and non-arrested HeLa cells revealed >4,100 and >2,200 residues either significantly phosphorylated or dephosphorylated, respectively, at mitotic entry. The calculated disorder scores of amino acid sequences of neighboring individual phosphosites revealed that >70% of dephosphorylated phosphosites exist in disordered regions, whereas 50% of phosphorylated sites exist in non-structured domains. A clear inverse correlation was observed between probability of phosphorylation in non-structured domain and increment of phosphorylation in mitosis. These results indicate that at entry to mitosis, a significant number of phosphate groups are removed from non-structured domains and transferred to more-structured domains. Gene ontology term analysis revealed that mitosis-related proteins are heavily phosphorylated, whereas RNA-related proteins are both dephosphorylated and phosphorylated, suggesting that heavy phosphorylation/dephosphorylation in non-structured domains of RNA-binding proteins plays a role in dynamic rearrangement of RNA-containing organelles, as well as other intracellular environments.

40 **Significance Statement**

41 Progression of mitosis is tightly regulated by protein phosphorylation/dephosphorylation. Although proteomic
42 studies have identified tens of thousands of phosphosites in mitotic cells, the roles of them remain to be
43 answered. We approached this question from the viewpoint of the higher-order structure of phosphosites.
44 Quantitative proteomics and bioinformatic analyses revealed that more than 70% of mitotic dephosphorylation
45 events occurred in non-structured regions. Non-structured regions of cellular proteins are attracting considerable
46 attention in terms of their involvement in dynamic rearrangements of intracellular membrane-less organelles
47 and protein assembly/disassembly processes. Our results suggest the possibility that a vast amount of mitosis-
48 associated dephosphorylation/phosphorylation at non-structured regions plays a role in regulating the dynamic
49 assembly/disassembly of intracellular architectures and organelles such as chromosomes and nucleolus.

50

Introduction

Protein phosphorylation/dephosphorylation plays a critical role in a number of cellular processes, such as intracellular signaling, cell cycle regulation, and mitosis. Studies using mass spectrometry have identified tens of thousands of phosphorylation sites, resulting in the creation of an atlas of phosphorylation states and dynamic alterations in phosphorylation during the cell cycle (1), mitosis (2–4), and cell differentiation and development (3, 4).

A variety of structural biological approaches have been used to elucidate the effect of phosphorylation on the structure/function of substrate proteins. The addition of a phosphate group to the hydroxyl group of a target residue (Ser, Thr, or Tyr) can affect i) interactions with other proteins, ii) access of substrate molecules to the catalytic center of the enzyme, or iii) local internal energy, which can exert allosteric effects on other parts of the protein. Phosphorylation significantly affects stereo-specific interactions between the substrate and other molecules, thus ensuring tight regulation of biological reactions.

Recent bioinformatics studies revealed that phosphorylation occurs preferentially on residues in intrinsically disordered regions (IDRs) of proteins (5–7). Due to the absence of secondary and tertiary structures, IDRs are thought to function as flexible substrates for both phosphorylation and other post-translational modifications (6). Although the structural and functional significance of IDR phosphorylation remains to be fully elucidated, several possibilities have been proposed. For example, the addition of a phosphate group could reduce the flexibility of the IDR, thus facilitating specific interactions. Phosphorylation of a serine residue in the IDR of the transcription factor Ets1 alters the structure of the IDR and reduces the affinity of Ets1 for DNA (8). Phosphorylation of Ser19 in the IDR of the regulatory light chain of smooth muscle myosin induces the formation of an α-helix that activates an actin-dependent ATPase (9–11).

Another possible role for phosphorylation of IDRs could be to reduce the stereo-specificity between kinases and substrates. The human genome encodes ~520 different kinases and ~150 phosphatases, which

74 phosphorylate and dephosphorylate, respectively, more than 40,000 sites in more than 10,000 proteins (12, 13).
75 A single kinase (or phosphatase) can therefore phosphorylate (or dephosphorylate) many different substrates.
76 Indeed, bioinformatic and biochemical studies have identified only weak consensus sequences for individual
77 kinases (14) and almost no consensus around the target residues of phosphatases. The presence of a target
78 residue in an IDR reduces the stereo-specificity of the enzyme-substrate interaction, thus enabling multiple
79 enzyme-substrate combinations.

80 Mitosis is a critical cellular process tightly regulated by phosphorylation. Several thousand protein
81 residues are known to be phosphorylated upon entry to mitosis (1, 2). A number of mitosis-associated kinases
82 have been identified, including CDK1, Aurora kinase, Plk1, Bub1, and Haspin (reviewed in [17–21]).
83 Dephosphorylation also plays an essential role during both mitotic entry and exit (22–25). More than 1,000
84 different phosphosites are known to be dephosphorylated during anaphase (22), and more than 500 are
85 dephosphorylated upon entry to mitosis (2). For example, CDK1 is activated via dephosphorylation by
86 Cdc25B/C (23, 24), and Cdc25C is partially activated by protein phosphatase 1 (23). These data indicate that a
87 vast number of phosphate groups are transferred to and from substrate proteins in the early phase of mitosis.

88 Several questions regarding mitotic phosphorylation that have yet to be answered include why and
89 how such a vast number of phosphate groups are transferred between different sets of proteins and whether
90 these different mitosis-associated phosphosites differ structurally. Determining the distribution of phosphosites
91 among structured and non-structured regions of substrate proteins is particularly important in terms of
92 understanding the structural effects of phosphorylation/dephosphorylation. In this study, we therefore
93 performed a phosphoproteomic analysis of cellular proteins to both quantify and compare individual
94 phosphosites in mitosis and interphase. We also analyzed the structural properties (i.e., IDR or structured) of
95 those sites. Our analysis of more than 6,000 phosphosites revealed a clear relationship between mitotic
96 phosphorylation/dephosphorylation and IDRs.

97

98 **Results**

99 **Quantitative proteomic analysis of phosphoproteins in mitosis**

100 A comparative proteomics analysis was performed to examine phosphopeptides obtained from asynchronous
101 and mitotic HeLa cells. Tryptic peptides from the two cell populations were labeled with tandem mass tag
102 (TMT) reagents. LC-MS/MS analysis was performed after enrichment of phosphopeptides using TiO_2. In total,
103 17,003 phosphopeptides were quantified (Fig. 1A), 15,368 of which were assigned to 3,701 proteins based on
104 database searching. For quantitative analysis of phosphorylation, peptides with only a single phosphosite were
105 extracted and assigned a mitotic abundance ratio, which provides an indication of enrichment in the specific
106 phosphosite in mitosis relative to interphase ($\log_2$[M phase/asynchronous]). For phosphosites detected in more
107 than two different peptides, the abundance ratio for each peptide was averaged. As a result, a total of 10,255
108 phosphorylation sites were quantified and subjected to further analyses, whereas 4,400 sites were detected only
109 in peptides with multiple phosphosites. Of 10,255 phosphorylation sites, 9,656 were already registered in the
110 PhophoSitePlus phosphoprotein database (25); thus, our dataset contained ≈600 previously unreported
111 phosphosites.

112 To extract phosphosites specifically up- or down-regulated during mitosis, the p-values for individual
113 peptides were plotted versus mitotic abundance. For a p-value threshold of 0.01 (Fig. 1A), two different
114 phosphosite populations were extracted, one positive in terms of mitotic abundance (UP group) and the other
115 negative (DOWN group) (Fig. 1B, Table S2). The UP group included 4,138 phosphosites distributed among
116 1,955 proteins, and the DOWN group included 2,249 phosphosites among 1,372 proteins. A significant number
117 of proteins (686) contained both UP and DOWN sites (Fig. 1C). A small peak found at ≈2.4 (mitotic abundance
118 ratio) (Fig. 1B) corresponded primarily to linker domains of C_2H_2 zinc finger proteins, which are known to be
119 phosphorylated during mitosis (26). Several mitotic phosphosites known to be up-regulated during mitosis, such

120 as S11 and S29 of histone H3.1 (27) and T161 of CDK1 (24), were identified in the UP group, with abundance
121 ratios of 2.4, 1.3, and 0.8, respectively. Phosphosite T14 of CDK1, known to be down-regulated during mitosis
122 (24), was detected in the DOWN group, with a mitotic abundance of −0.7.

123 Gene ontology (GO) analysis was performed for the UP and DOWN sites. Using DAVID, we
124 obtained biological process terms (28, 29) and evaluated GO term enrichment in each group by dividing the
125 number of proteins by the total number of proteins associated with specific GO terms (Fig. 1D). As expected,
126 the UP sites were highly enriched in proteins related to mitotic chromosomes. Interestingly, both UP and DOWN
127 sites were highly enriched in proteins related to RNA processing and splicing, suggesting that RNA-related
128 proteins are regulated by both phosphorylation and dephosphorylation during mitosis (see *Discussion* section).

129 A larger number of UP sites than DOWN sites does not necessarily mean that there is a greater
130 amount of phosphorylated proteins than dephosphorylated proteins in a mitotic cell. To examine this issue
131 further, the phosphorylated proteins in cells in interphase and mitosis were quantified by dot-blot analysis using
132 pIMAGO (30). Careful quantification revealed that 5.4 fmol of phosphate groups were attached to proteins in a
133 single mitotic cell, versus 3.8 fmol in an asynchronous cell. These values correspond to 4.7 and 3.3 mM in the
134 mitotic and asynchronous cells, respectively (the volume of a HeLa cell is reportedly 1.16 pL [35]) (Fig. S1A),
135 indicating that mitotic cells contain 1.4 times more phosphate groups on proteins than asynchronous cells. These
136 results were consistent with an observed decrease in the ATP concentration as determined using a FRET probe
137 (Fig. S1B, C, D) (32, 33), and this decrease was inhibited by the universal kinase inhibitor staurosporine (Fig.
138 S2A, B). The reduction in the ATP concentration was not due to cell swelling during mitosis (34, 35) (Fig. S1E),
139 rearrangement of the actin cytoskeleton (Fig. S2C, D), or a decrease in the ATP supply (glycolysis and oxidative
140 phosphorylation) (Fig. S2E-H). These results indicate that although both phosphorylation and
141 dephosphorylation occur during mitosis, phosphorylation is the dominant process.

142

143 **Mitotic dephosphorylation occurs preferentially in non-structured regions**

144 The relationship between mitosis-specific phosphorylation/dephosphorylation and the higher-order structure of
145 polypeptides was also investigated. A previous study reported that phosphorylation of substrate proteins tends
146 to occur in non-structured regions (IDRs) (5). We therefore evaluated the intrinsic disorder score of individual
147 residues using the IUPred method (36, 37). In this study, the minimum length of the IDR was set to 30 amino
148 acid residues (see *Materials and Methods*). Using this criterion, 23.4% of Ser/Thr residues among all cellular
149 proteins are present in IDRs (Fig. 2A). In contrast, 59.6% of the 10,255 phosphosites quantified in our proteomic
150 analysis were assigned in IDRs (Fig. 2A), demonstrating the strong likelihood of phosphorylation occurring in
151 IDRs. As a comparison, other post-translational modifications were also subjected to the same analysis. As
152 shown in Figure S3, the probabilities of ubiquitylation, methylation and acetylation sites existing in IDRs were
153 lower than that of phosphorylation, confirming that this likelihood is specific to phosphorylation and not general
154 tendency of post-translational modifications.

155 We then examined the relationship between mitotic phosphorylation/dephosphorylation and IDRs.
156 As shown in Figure 2A, 71.0% of DOWN and 52.6% of UP sites were found in IDRs. Interestingly, a strong
157 inverse correlation between abundance ratio and IDR probability was found; the IDR probability gradually
158 decreased from ~80 to 40% with increasing abundance ratio (Fig. 2B). These values were extremely high
159 compared to the average for all Ser/Thr residues (23.4%). Collectively, these results demonstrate that
160 phosphorylation generally occurs preferentially in IDRs, and this is particularly and significantly true for
161 dephosphorylation upon entry to mitosis.

162 The specific phosphosite amino acid residue was also strongly correlated with the mitotic abundance
163 ratio. As shown in Figure 2C, >90% of DOWN sites involved Ser, versus only ~7.8% for Thr residues. The
164 percentage of Ser residues decreased as the mitotic abundance increased; 75.2% of UP sites were Ser, and 24.8%
165 were Thr, indicating that mitotic dephosphorylation occurs primarily at Ser residues, whereas mitotic

166 phosphorylation occurs at both at Ser and Thr residues. These results could be explained at least in part by the
167 strong correlation between IDRs and DOWN sites, as Ser has a higher disorder probability than Thr.
168 Alternatively, this could be associated with phosphatase preference. PP2A is known to prefer Thr over Ser and
169 be inactivated at mitosis entry and re-activated in anaphase, as demonstrated previously (21, 22, 38, 39) (see
170 *Discussion*).
171
172 **Mitotic phosphorylation–specific non-conventional sequence motifs**
173 Next, we analyzed the sequence motifs specific to the UP and DOWN phosphosites. The UP and DOWN
174 phosphosites were assigned as one of the following consensus sequences based on their flanking amino acids
175 (from −6 to +6): "proline-directed" ([pS/pT]-P), phosphorylated by CDK and MAPK; "acidophilic" ([pS/pT]-
176 X-X-[D/E], [pS/pT]-X-[D/E] or [D/E]-X-[pS/pT]), recognized by PLK1 and casein kinase; "basophilic" ([K/R]-
177 X-X-[pS/pT] or [K/R]-X-[pS/pT]), phosphorylated by Aurora kinase, PKC, and PKA (2, 40); and "non-
178 conventional" for those that did not match any of the three above categories.
179 As shown in Figure 3A and B, three conventional motifs ("proline-directed", "acidophilic", and
180 "basophilic") constituted 92.3% of DOWN sites, indicating that most mitotic dephosphorylation occurs at one
181 of these conventional motifs. Interestingly, the amount of phosphorylation occurring at non-conventional motifs
182 was higher for UP sites than DOWN sites (Figs. 3A and S4), suggesting the possibility of a mitosis-specific
183 non-conventional motif. The conventional and non-conventional motifs also exhibited a clear contrast with
184 regard to the relationship between the probability of phosphosites in IDR and mitotic abundance. As shown in
185 Figure 3C, the probability of an IDR was inversely correlated with the mitotic abundance ratio for all three
186 conventional motifs, as demonstrated in Figure 2A. In a clear contrast, the IDR probability in non-conventional
187 motifs increased with increasing abundance ratio (Fig. 3C). The high IDR probability of UP sites was opposite
188 to that of the conventional motifs. These results suggest that non-conventional motifs in IDRs are

189 phosphorylated upon entry to mitosis.

190 We then analyzed the amino acid sequences of "non-conventional" motifs. Logo analysis of 557 UP
191 phospho-serine and 79 UP phospho-threonine sites in non-conventional motifs revealed a high frequency of
192 basic residues (Lys or Arg) on the carboxylic side (+2 to +6) of the phosphosite (Fig. 3D). The presence of K/R
193 at the +3 position was particularly notable. In contrast, no clear consensus was found regarding the amino-
194 terminal side of the phosphosites, except for a weak consensus of a hydrophobic residue at the −2 position and
195 K/R at the −6 position. This consensus was found to be distinct from any other known kinase motifs, including
196 the conventional basophilic motif, which consists of a basic amino acid at the −2 or −3 position. In a clear
197 contrast, no such consensus was found with respect to the DOWN sites; with no clear consensus for the 133
198 DOWN phospho-serine and 20 DOWN phospho-threonine sites in the non-conventional motifs (Fig. 3E). These
199 results suggest that the non-conventional basophilic motifs (Non-conventional basic residues at carboxylic side
200 motif (NBC motif)) are unique mitosis-specific phosphorylation sites.

201 GO term analyses were conducted for proteins carrying an UP site in the non-conventional motif
202 (502 proteins). In contrast to the results of GO term analyses of all phosphoproteins with an UP site, proteins
203 related to "mRNA export from the nucleus" were highly enriched in NBC motifs (24 of 502 proteins with non-
204 conventional motifs [4.8%] vs. 50 of all 1,955 proteins with UP sites [2.6%]) (Fig. 3F). These proteins contain
205 subunits of the nuclear pore complex (Nups), splicing factors, and other RNA-binding proteins. Nups and
206 proteins with transcription regulator activity are known to carry a substantial number of IDRs (41, 42). These
207 results, together with those regarding dephosphorylation of RNA-related proteins (Fig. 1D), suggest that
208 phosphorylation/dephosphorylation of RNA-related proteins play important roles in the progression of mitosis.

209

210 **Discussion**

211 In this study, we conducted a comparative proteomic analysis of amino acid residues phosphorylated in cells

212 undergoing mitosis and interphase cells using a TMT-6plex labeling technique that provides a ratio of the
213 amounts of individual peptides in six samples with high precision (43). Using this approach, we extracted two
214 different populations of phosphopeptides, one up-regulated and the other down-regulated upon entry to mitosis.
215 Bioinformatic analyses of these phosphopeptides revealed a clear correlation between
216 phosphorylation/dephosphorylation and the IDR probability of the substrate. The most striking outcome of our
217 analysis was that although phosphorylation generally tends to occur in IDRs, this trend is more common with
218 mitotic dephosphorylation, as >70% of DOWN sites were found in IDRs, versus only 50% of UP sites (Fig. 2A,
219 B). These data indicate that a significant number of phosphate groups are removed from IDRs and introduced
220 into more structured regions upon entry to mitosis. Although we did not elucidate the significance of this
221 translocation of phosphate groups from IDRs to structured regions in this study, several intriguing clues can be
222 discerned from analyses of flanking amino acid sequences and GO term analysis: i) most mitotic
223 dephosphorylation occurs at Ser residues (91.9 %), whereas phosphorylation occurs at both Ser and Thr residues
224 (75.2%, 24.8%, respectively) (Fig. 2C); ii) proteins involved in mitotic chromosome segregation are heavily
225 phosphorylated, whereas proteins related to RNA splicing and metabolism are both dephosphorylated and
226 phosphorylated (Fig. 1D); and iii) non-conventional basic motifs are preferentially phosphorylated during
227 mitosis (Fig. 3A, D, E). These intriguing results suggest a correlation between mitotic phosphorylation and
228 dynamic higher-order assembly/disassembly of biomolecules (proteins, DNA, and RNA). Below, we discuss
229 the potential significance of such dynamic behavior of biomolecules in the context of cellular function.

230 One effect of phosphorylation in IDRs could be to facilitate the transition of higher-order structures
231 (8, 44, 45). Phosphorylation in IDRs is known to cause disordered-to-ordered and ordered-to-disordered
232 transitions. For example, phosphorylation of 4E-BP2 induces the formation of a four-stranded β-sheet, thus
233 preventing the binding of eIF4E (46). Phosphorylation of phospholamban at Ser16, in contrast, disrupts the
234 higher-order structure, in turn reducing the inhibitory effect of phospholamban on sarco(endo)plasmic Ca-

235 ATPase activity (47, 48).

236 Another possible role for phosphorylation in IDRs is regulation of the phase transition of
237 biomolecules. Non-structured polypeptides of IDRs have been demonstrated to play key roles in liquid-liquid
238 phase separation (49). It is driven by a number of promiscuous interactions to assemble a number of molecules.
239 Other studies demonstrated that phase transition of protein liquid droplets is induced by
240 phosphorylation/dephosphorylation (50–52). For example, liquid-liquid phase separation of a complex of a
241 positively charged artificial peptide and RNA is promoted by dephosphorylation of the peptide (53). A study
242 using a short hydrophobic peptide that forms a hydrogel demonstrated that reversible gel-sol transition is
243 induced by cyclic phosphorylation-dephosphorylation by kinases and phosphatases (54). The peptide hydrogel
244 is transformed into solution upon addition of kinase and ATP to the gel and re-solidifies when phosphatase is
245 added to the solution. Such phenomena have also been observed in living cells. The assembly/disassembly of
246 RNA granules is regulated by phosphorylation/dephosphorylation of one of the subunits (55). Although the
247 mechanism is not fully understood, available evidence suggests a possible effect of
248 phosphorylation/dephosphorylation on the dynamic assembly/disassembly transition of biomolecules upon
249 entry to mitosis. It is possible that phosphate groups in IDRs function in weakly assembling the proteins during
250 interphase, and their removal (dephosphorylation) could induce final assembly of the proteins into a stable
251 complex. Alternatively, mitotic phosphorylation could solubilize/disassemble the protein complex, and
252 dephosphorylation during anaphase could reassemble the complex. Indeed, phosphorylation of proteins in
253 splicing speckles, pericentriolar-satellites, and stress granule by DYRK3 results in disassembly of these
254 membrane-less organelles during mitosis (56). Such phosphorylation-dependent regulation of protein
255 assembly/disassembly depends on the sequence of amino acid residues flanking the substrate residue. A
256 previous report demonstrated that the charge pattern—rather than the net charge—is most important for phase
257 separation (57). The addition of a negative charge due to phosphorylation could enhance or disrupt the charge

258 pattern and thus affect the progress of phase separation.

259 Our GO term analysis of UP and DOWN phosphosites revealed that RNA-related proteins are
260 preferentially dephosphorylated and phosphorylated during mitosis (Fig. 1D). This result is intriguing in the
261 context of phosphorylation-dependent regulation of phase transition in intracellular compartments. A recent
262 study demonstrated that the structure and function of several intracellular compartments are maintained by
263 phase separation, in which RNA plays a role in the molecular assembly (58). P-granules are cytoplasmic
264 compartments in the germ line of *C. elegans*, and they are considered liquid-like condensates containing mRNA
265 and RNA-binding proteins that function in posttranscriptional regulation (59, 60). Protein components of P
266 granules, such as PGL-3 and LAF-1, form liquid droplets *in vitro*, and mRNA affects the dynamics of these
267 proteins within the droplets (64, 65). In the nucleolus, which is also considered a compartment, proteins and
268 RNAs assemble via a mechanism similar to phase separation (63). The nucleolar protein nucleophosmin forms
269 droplets with rRNA *in vitro* (64). Phosphorylation of $Thr^{199, 219, 234, 237}$ by CDK1 reduces the affinity for rRNA
270 (65), and replacement of these Ser residues with Glu partially abolishes nucleolar localization in HeLa cells
271 (66), suggesting that phosphorylation of nucleophosmin controls the dynamics of proteins and RNAs within the
272 nucleolus. It is possible that the removal/addition of a large number of phosphate groups from/to IDRs of RNA-
273 related proteins induces dynamic rearrangements of the nucleolus and other RNA-containing nuclear speckles
274 upon entry to mitosis, resulting in disruption of these organelles and the release of a large number of RNA
275 molecules into the cytoplasm. This would dramatically alter the intracellular environment and could affect the
276 assembly/disassembly dynamics of other protein complexes, such as chromosomes, which are known to contain
277 pre-ribosomal RNA and nucleolar proteins on the surface (67, 68). It is also possible that chromosome
278 condensation could be induced by the orchestrated effects of phosphorylation of chromosome-related proteins
279 (Fig. 1D) and dramatic RNA-induced changes in the intracellular environment. Further study will be required
280 to resolve this issue.

281 An unexpected result of the present study was that most dephosphorylation upon entry to mitosis
282 was found to occur at Ser residues, whereas phosphorylation was found to occur at both Ser and Thr residues
283 (Fig. 2C), suggesting that Thr phosphorylation is a mitosis-specific event. It is possible that such Thr
284 phosphorylation of substrate proteins is coupled with dephosphorylation during anaphase and therefore
285 temporary during early mitosis. There are several lines of experimental evidence that support this possibility: i)
286 dephosphorylation during anaphase and telophase occur preferentially at Thr residues in HeLa cells (22, 38); ii)
287 in budding yeast, Thr residues are heavily phosphorylated upon entry to mitosis and dephosphorylated during
288 anaphase by $PP2A^{Cdc55}$, an orthologue of $PP2A^{B55}$ (21, 39, 69); iii) biochemical analyses revealed that $PP2A^{B55}$,
289 a major anaphase-associated phosphatase, preferentially dephosphorylates Thr residues over Ser residues (70);
290 and iv) a comparison of our dataset of UP sites with a previously reported dephosphorylation dataset (22)
291 revealed that 29.9% of Thr and 9.4% of Ser residues detected in the both datasets are dephosphorylated during
292 anaphase. These data suggest that Thr phosphorylation during mitosis is temporary and functions to regulate
293 reactions that are tightly tuned temporally during mitosis. The combined activities of kinases and phosphatases
294 enable such tight regulation. Although the structural background of Thr-specific reactions has yet to be
295 elucidated, it must be involved in early mitotic events such as chromosome condensation.

296 We identified mitosis-specific phosphorylation motifs similar to conventional basophilic motifs but
297 different in the position of basic residues (Fig. 3D). Although distinct from any known phosphorylation motifs,
298 several candidates were found in a phosphoproteomic database (2). PKC is known to function in mitosis (71,
299 72) and phosphorylate Ser residues near basic amino acids. However, the consensus sequences of several PKC
300 subtypes contain basic residues on the C-terminal side as well (40). PKCε plays a role in resolving mitotic DNA
301 catenation (73). Our GO term analysis revealed that proteins related to sister chromatid segregation are enriched
302 in proteins carrying NBC motifs. Another potential candidate is AMPK, which is activated when AMP levels
303 increase and ATP levels decrease (74) and known to phosphorylate mitosis-related proteins (75). Although the

304 primary consensus motif for AMPK is basophilic, a peptide with K/R at the +3 position, which is the same as
305 the NBC motif, is also phosphorylated *in vitro* (76). Of 243 proteins identified as substrates of AMPK to date
306 (75), 17.3% (42 proteins) were found to contain UP sites in the NBC motif in our study (Table S2). Furthermore,
307 it is intriguing that the intracellular ATP level decreased during early mitosis (Fig. S1B-D). These results suggest
308 that mitosis is regulated by an ATP-dependent regulatory mechanism; decreasing intracellular ATP levels
309 resulting from the activity of conventional kinases upon entry to mitosis may activate AMPK, which then
310 phosphorylates different sets of substrate proteins to induce the progression of mitosis. The activity of AMPK
311 increases during early mitosis and then decreases when cytokinesis begins (75), in good agreement with
312 observed ATP levels during mitosis (Fig. S1C).
313

314 **Materials and Methods**

315 **Cell culture and synchronization**

316 HeLa cells were cultured in Dulbecco's modified eagle medium (DMEM) (Sigma-Aldrich) with 10% fetal
317 bovine serum (FBS) (GIBCO) at 37°C and 5% CO_2. For mitosis-arrested cells, cells were treated first with 2
318 mM thymidine (Sigma-Aldrich) for 18 h, washed with PBS, and released into DMEM with 10% FBS for 1 h.
319 Following treatment with 0.2 μM nocodazole for 10 h, 80% synchronization of HeLa cells in mitosis was
320 achieved.
321

322 **TMT labeling and mass spectrometry**

323 Asynchronous and mitosis-arrested HeLa cells in 100-mm cell culture dishes (Corning) were washed twice with
324 5 mL of ice-cold Hepes-saline (20 mM Hepes-NaOH [pH 7.5], 137 mM NaCl). Next, 0.75 mL of guanidine
325 hydrochloride buffer (6 M guanidine hydrochloride, 100 mM Tris-HCl [pH 8.0], 2 mM DTT) was added, and
326 cell lysates were prepared in triplicate and frozen in liquid nitrogen. The lysates were dissolved by heating and

327 sonication, followed by centrifugation at 20,000 × *g* for 15 min at 4°C. The supernatants were reduced in 5 mM
328 DTT at room temperature for 30 min and alkylated in 27.5 mM iodoacetamide at room temperature for 30 min
329 in the dark. Proteins were purified by methanol/chloroform precipitation and solubilized by addition of 25 µL
330 of 0.1% RapiGest SF (Waters) in 50 mM triethylammonium bicarbonate. After repeated sonication and
331 vortexing, the proteins were digested with 2 µg of trypsin/Lys-C mix (Promega) for 16 h at 37°C. The peptide
332 concentration was determined using a Pierce quantitative colorimetric peptide assay (Thermo Fisher Scientific).
333 Approximately 150 µg of peptides for each sample was labeled with 200 µg of TMT-6plex reagent (Thermo
334 Fisher Scientific) for 1 h at room temperature. After the reaction was quenched with hydroxylamine, all TMT-
335 labeled samples were pooled and acidified with trifluoroacetic acid (TFA). Phosphopeptides were enriched
336 using a 50-mg column of Titansphere Phos-TiO (GL Sciences) in accordance with the manufacturer's
337 instructions and then fractionated using a Pierce high-pH reversed-phase peptide fractionation kit (Thermo
338 Fisher Scientific). Eight fractions were collected: 5, 7.5, 10, 12.5, 15, 17.5, 20, and 50% acetonitrile. Each
339 fraction was evaporated in a SpeedVac concentrator and dissolved in 0.1% TFA.
340

341 **Data analysis**

342 Data analysis was performed using Python2 or 3 and the accompanying libraries (Numpy, Scipy, Pandas,
343 Matplotlib, Seaborn) using Jupyter (IPython) Notebook. The latest version of the phosphosites dataset from
344 PhosphoSitePlus (25) (Wed Nov 08 15:57:30 EST 2017) was used. For GO term analysis, DAVID 6.8 (28, 29)
345 was used. The term "BP_5" was obtained as a biological process term applying *Homo sapiens* as the background.
346 The number of proteins in our dataset was divided by the total number of proteins for each GO term to evaluate
347 the abundance of the term. For IDR analysis, the IUPred method (36, 37) was used. Position-specific estimations
348 of energies of each residue were calculated based on the method described by Dosztányi using Perl script.
349 Residues with an energy greater than −0.203 [aeu] were defined as intrinsically disordered residues according

350 to the IUPred method. Contiguous amino acid sequences of more than 30 intrinsically disordered residues were
351 regarded as intrinsically disordered regions. LOGO analysis of the neighboring amino acids of phosphosites
352 was performed using the "PSP production" algorithm in PhosphoSitePlus (25).
353
354 **Acknowledgments**
355 This study was supported financially by The Sumitomo Foundation Grant for Basic Science Research Projects
356 (Grant Number 150852) for S.H.Y and JSPS Grant-in-Aid for JSPS Fellows (Grant Number 17J09002) for H.Y.
357 We thank T. Oda for the assistance in the analysis of IDR.
358
359
360

361 1. J. V Olsen, M. Vermeulen, A. Santamaria, C. Kumar, M.L. Miller, L.J. Jensen, et al., Quantitative
362 phosphoproteomics reveals widespread full phosphorylation site occupancy during mitosis. *Sci Signal*.
363 **3**, ra3 (2010).
364 2. N. Dephoure, C. Zhou, J. Villen, S.A. Beausoleil, C.E. Bakalarski, S.J. Elledge, et al., A quantitative
365 atlas of mitotic phosphorylation. *Pnas*. **105**, 10762–10767 (2008).
366 3. J. Yue, X. Gou, P. Lee, M. Schober, X. Wu, M. Tan, et al., Phosphorylation of Pkp1 by RIPK4
367 regulates epidermal differentiation and skin tumorigenesis. *EMBO J*. **36**, 1963–1980 (2017).
368 4. M.M. Roux, M.J. Radeke, M. Goel, A. Mushegian, K.R. Foltz, 2DE identification of proteins
369 exhibiting turnover and phosphorylation dynamics during sea urchin egg activation. *Dev Biol*. **313**,
370 630–647 (2008).
371 5. L.M. Iakoucheva, P. Radivojac, C.J. Brown, T.R. O'Connor, J.G. Sikes, Z. Obradovic, et al., The
372 importance of intrinsic disorder for protein phosphorylation. *Nucleic Acids Res*. **32**, 1037–1049 (2004).
373 6. A.L. Darling, V.N. Uversky, Intrinsic disorder and posttranslational modifications: The darker side of
374 the biological dark matter. *Front Genet*. **9**, 1–18 (2018).
375 7. M.O. Collins, L. Yu, I. Campuzano, S.G.N. Grant, J.S. Choudhary, Phosphoproteomic Analysis of the
376 Mouse Brain Cytosol Reveals a Predominance of Protein Phosphorylation in Regions of Intrinsic
377 Sequence Disorder. *Mol Cell Proteomics*. **7**, 1331–1348 (2008).
378 8. K. Kasahara, M. Shiina, J. Higo, K. Ogata, H. Nakamura, Phosphorylation of an intrinsically
379 disordered region of Ets1 shifts a multi-modal interaction ensemble to an auto-inhibitory state. *Nucleic*
380 *Acids Res*. **46**, 2243–2251 (2018).
381 9. W.D. Nelson, S.E. Blakely, Y.E. Nesmelov, D.D. Thomas, Site-directed spin labeling reveals a
382 conformational switch in the phosphorylation domain of smooth muscle myosin. *Proc Natl Acad Sci*.
383 **102**, 4000–4005 (2005).

384 10. L.M. Espinoza-Fonseca, D. Kast, D.D. Thomas, Molecular dynamics simulations reveal a disorder-to-
385 order transition on phosphorylation of smooth muscle myosin. *Biophys J*. **93**, 2083–2090 (2007).
386 11. L.M. Espinoza-Fonseca, D. Kast, D.D. Thomas, Thermodynamic and structural basis of
387 phosphorylation-induced disorder-to-order transition in the regulatory light chain of smooth muscle
388 myosin. *J Am Chem Soc*. **130**, 12208–12209 (2008).
389 12. F. Ardito, M. Giuliani, D. Perrone, G. Troiano, L. Lo Muzio, The crucial role of protein
390 phosphorylation in cell signalingand its use as targeted therapy (Review). *Int J Mol Med*. **40**, 271–280
391 (2017).
392 13. H. Horn, E.M. Schoof, J. Kim, X. Robin, M.L. Miller, F. Diella, et al., KinomeXplorer: An integrated
393 platform for kinome biology studies. *Nat Methods*. **11**, 603–604 (2014).
394 14. H.L. Rust, P.R. Thompson, Kinase consensus sequences: A breeding ground for crosstalk. *ACS Chem*
395 *Biol*. **6**, 881–892 (2011).
396 15. F. Bazile, J. St-Pierre, D. D'Amours, Three-step model for condensin activation during mitotic
397 chromosome condensation. *Cell Cycle*. **9**, 3243–3255 (2010).
398 16. G. Wang, Q. Jiang, C. Zhang, The role of mitotic kinases in coupling the centrosome cycle with the
399 assembly of the mitotic spindle. *J Cell Sci*. **127**, 4111–4122 (2014).
400 17. R. Bayliss, A. Fry, T. Haq, S. Yeoh, On the molecular mechanisms of mitotic kinase activation. *Open*
401 *Biol*. **2**, 120136–120136 (2012).
402 18. E.A. Nigg, Mitotic kinases as regulators of cell division and its checkpoints. *Nat Rev Mol Cell Biol*. **2**,
403 21–32 (2001).
404 19. M. Alvarez-Fernandez, M. Malumbres, Preparing a cell for nuclear envelope breakdown: Spatio-
405 temporal control of phosphorylation during mitotic entry. *BioEssays*. **36**, 757–765 (2014).
406 20. F.A. Barr, P.R. Elliott, U. Gruneberg, Protein phosphatases and the regulation of mitosis. *J Cell Sci*.

407 **124**, 2323–2334 (2011).

408 21. H. Kim, G. Fernandes, C. Lee, Protein Phosphatases Involved in Regulating Mitosis: Facts and
409 Hypotheses. *Mol Cells*. **39**, 654–62 (2016).

410 22. A. Castro, R.A. McCloy, S. Rogers, N.J. Hoffman, B.L. Parker, T. Lorca, et al., Global
411 Phosphoproteomic Mapping of Early Mitotic Exit in Human Cells Identifies Novel Substrate
412 Dephosphorylation Motifs. *Mol Cell Proteomics*. **14**, 2194–2212 (2015).

413 23. E. Perdiguero, A.R. Nebreda, Regulation of Cdc25C activity during the meiotic G2/M transition. *Cell*
414 *Cycle*. **3**, 733–737 (2004).

415 24. O. Timofeev, O. Cizmecioglu, F. Settele, T. Kempf, I. Hoffmann, Cdc25 phosphatases are required for
416 timely assembly of CDK1-cyclin B at the G2/M transition. *J Biol Chem*. **285**, 16978–16990 (2010).

417 25. P. V. Hornbeck, B. Zhang, B. Murray, J.M. Kornhauser, V. Latham, E. Skrzypek, PhosphoSitePlus,
418 2014: Mutations, PTMs and recalibrations. *Nucleic Acids Res*. **43**, D512–D520 (2015).

419 26. R. Rizkallah, K.E. Alexander, M.M. Hurt, Global mitotic phosphorylation of C2H2 zinc finger protein
420 linker peptides. *Cell Cycle*. **10**, 3327–3336 (2011).

421 27. C. Crosio, G.M. Fimia, R. Loury, Y. Okano, H. Zhou, S. Sen, et al., Mitotic Phosphorylation of
422 Histone H3 : Spatio-Temporal Regulation by Mammalian Aurora Kinases. **22**, 874–885 (2002).

423 28. D.W. Huang, B.T. Sherman, R.A. Lempicki, Systematic and integrative analysis of large gene lists
424 using DAVID bioinformatics resources. *Nat Protoc*. **4**, 44–57 (2009).

425 29. D.W. Huang, B.T. Sherman, R.A. Lempicki, Bioinformatics enrichment tools: Paths toward the
426 comprehensive functional analysis of large gene lists. *Nucleic Acids Res*. **37**, 1–13 (2009).

427 30. L. Pan, L. Wang, C.-C. Hsu, J. Zhang, A. Iliuk, W.A. Tao, Sensitive measurement of total protein
428 phosphorylation level in complex protein samples. *Analyst*. **140**, 3390–3396 (2015).

429 31. A. Fujioka, K. Terai, R.E. Itoh, K. Aoki, T. Nakamura, S. Kuroda, et al., Dynamics of the Ras/ERK

430 MAPK cascade as monitored by fluorescent probes. *J Biol Chem*. **281**, 8917–8926 (2006).

431 32. E. Ahn, P. Kumar, D. Mukha, A. Tzur, T. Shlomi, Temporal fluxomics reveals oscillations in TCA
432 cycle flux throughout the mammalian cell cycle. *Mol Syst Biol*. **13**, 953 (2017).

433 33. K. Maeshima, T. Matsuda, Y. Shindo, H. Imamura, S. Tamura, R. Imai, et al., A Transient Rise in Free
434 Mg 2+ Ions Released from ATP-Mg Hydrolysis Contributes to Mitotic Chromosome Condensation.
435 *Curr Biol*. 1–8 (2018).

436 34. S. Son, J.H. Kang, S. Oh, M.W. Kirschner, T.J. Mitchison, S. Manalis, Resonant microchannel volume
437 and mass measurements show that suspended cells swell during mitosis. *J Cell Biol*. **211**, 757–763
438 (2015).

439 35. E. Zlotek-Zlotkiewicz, S. Monnier, G. Cappello, M. Le Berre, M. Piel, Optical volume and mass
440 measurements show that mammalian cells swell during mitosis. *J Cell Biol*. **211**, 765–774 (2015).

441 36. Z. Dosztányi, V. Csizmók, P. Tompa, I. Simon, The pairwise energy content estimated from amino
442 acid composition discriminates between folded and intrinsically unstructured proteins. *J Mol Biol*. **347**,
443 827–839 (2005).

444 37. Z. Dosztányi, V. Csizmok, P. Tompa, I. Simon, IUPred: Web server for the prediction of intrinsically
445 unstructured regions of proteins based on estimated energy content. *Bioinformatics*. **21**, 3433–3434
446 (2005).

447 38. R. Malik, R. Lenobel, A. Santamaria, A. Ries, E.A. Nigg, R. Körner, Quantitative analysis of the
448 human spindle phosphoproteome at distinct mitotic stages. *J Proteome Res*. **8**, 4553–4563 (2009).

449 39. M. Godfrey, S.A. Touati, M. Kataria, A. Jones, A.P. Snijders, F. Uhlmann, PP2ACdc55 Phosphatase
450 Imposes Ordered Cell-Cycle Phosphorylation by Opposing Threonine Phosphorylation. *Mol Cell*. **65**,
451 393-402.e3 (2017).

452 40. A. Kreegipuu, N. Blom, S. Brunak, J. Ja, Statistical analysis of protein kinase specifcity determinants.

453 *FEBS Lett*. **430**, 45–50 (1998).

454 41. S.S. Patel, D.P. Denning, A.L. Fink, V. Uversky, M. Rexach, Disorder in the nuclear pore complex:
455 The FG repeat regions of nucleoporins are natively unfolded. *Proc Natl Acad Sci*. **100**, 2450–2455
456 (2003).

457 42. C. Haynes, C.J. Oldfield, F. Ji, N. Klitgord, M.E. Cusick, P. Radivojac, et al., Intrinsic disorder is a
458 common feature of hub proteins from four eukaryotic interactomes. *PLoS Comput Biol*. **2**, 0890–0901
459 (2006).

460 43. A. Hogrebe, L. Von Stechow, D.B. Bekker-Jensen, B.T. Weinert, C.D. Kelstrup, J. V. Olsen,
461 Benchmarking common quantification strategies for large-scale phosphoproteomics. *Nat Commun*. **9**,
462 (2018). doi:10.1038/s41467-018-03309-6.

463 44. T. Travers, H. Shao, B.A. Joughin, D.A. Lauffenburger, A. Wells, C.J. Camacho, Tandem
464 phosphorylation within an intrinsically disordered region regulates ACTN4 function. *Sci Signal*. **8**, 1–
465 10 (2015).

466 45. M.E. Fealey, B.P. Binder, V.N. Uversky, A. Hinderliter, D.D. Thomas, Structural Impact of
467 Phosphorylation and Dielectric Constant Variation on Synaptotagmin's IDR. *Biophys J*. **114**, 550–561
468 (2018).

469 46. A. Bah, R.M. Vernon, Z. Siddiqui, M. Krzeminski, R. Muhandiram, C. Zhao, et al., Folding of an
470 intrinsically disordered protein by phosphorylation as a regulatory switch. *Nature*. **519**, 106–9 (2015).

471 47. E.E. Metcalfe, N.J. Traaseth, G. Veglia, Serine 16 phosphorylation induces an order-to-disorder
472 transition in monomeric phospholamban. *Biochemistry*. **44**, 4386–4396 (2005).

473 48. G. Chu, E.G. Kranias, Functional interplay between dual site phospholambam phosphorylation:
474 insights from genetically altered mouse models. *Basic Res Cardiol*. **97**, 1–1 (2003).

475 49. V.N. Uversky, Intrinsically disordered proteins in overcrowded milieu: Membrane-less organelles,

476 phase separation, and intrinsic disorder. *Curr Opin Struct Biol*. **44**, 18–30 (2017).

477 50. I. Kwon, M. Kato, S. Xiang, L. Wu, P. Theodoropoulos, H. Mirzaei, et al., Phosphorylation-regulated
478 binding of RNA polymerase ii to fibrous polymers of low-complexity domains. *Cell*. **156**, 374 (2014).

479 51. J. Guillén-Boixet, V. Buzon, X. Salvatella, R. Méndez, CPEB4 is regulated during cell cycle by
480 ERK2/Cdk1-mediated phosphorylation and its assembly into liquid-like droplets. *Elife*. **5**, 1–26 (2016).

481 52. Z. Monahan, V.H. Ryan, A.M. Janke, K.A. Burke, S.N. Rhoads, G.H. Zerze, et al., Phosphorylation of
482 the FUS low-complexity domain disrupts phase separation, aggregation, and toxicity. *EMBO J*. **36**,
483 e201696394 (2017).

484 53. W.M. Aumiller, C.D. Keating, Phosphorylation-mediated RNA/peptide complex coacervation as a
485 model for intracellular liquid organelles. *Nat Chem*. **8**, 129–137 (2016).

486 54. Z. Yang, G. Liang, L. Wang, B. Xu, Using a kinase/phosphatase switch to regulate a supramolecular
487 hydrogel and forming the supramolecular hydrogel in vivo. *J Am Chem Soc*. **128**, 3038–3043 (2006).

488 55. J.T. Wang, J. Smith, B.C. Chen, H. Schmidt, D. Rasoloson, A. Paix, et al., Regulation of RNA granule
489 dynamics by phosphorylation of serine-rich, intrinsically disordered proteins in C. elegans. *Elife*. **3**, 1–
490 23 (2014).

491 56. A.K. Rai, J.X. Chen, M. Selbach, L. Pelkmans, Kinase-controlled phase transition of membraneless
492 organelles in mitosis. *Nature*. **559**, 211–216 (2018).

493 57. T.J. Nott, E. Petsalaki, P. Farber, D. Jervis, E. Fussner, A. Plochowietz, et al., Phase Transition of a
494 Disordered Nuage Protein Generates Environmentally Responsive Membraneless Organelles. *Mol*
495 *Cell*. **57**, 936–947 (2015).

496 58. Y. Lin, D.S.W. Protter, M.K. Rosen, R. Parker, Formation and Maturation of Phase-Separated Liquid
497 Droplets by RNA-Binding Proteins. *Mol Cell*. **60**, 208–219 (2015).

498 59. D. Updike, S. Strome, P granule assembly and function in Caenorhabditis elegans germ cells. *J Androl*.

499 **31**, 53–60 (2010).

500 60. G. Seydoux, The P Granules of C. elegans: A Genetic Model for the Study of RNA–Protein
501 Condensates. *J Mol Biol*. **430**, 4702–4710 (2018).

502 61. S. Saha, C.A. Weber, M. Nousch, O. Adame-Arana, C. Hoege, M.Y. Hein, et al., Polar Positioning of
503 Phase-Separated Liquid Compartments in Cells Regulated by an mRNA Competition Mechanism.
504 *Cell*. **166**, 1572-1584.e16 (2016).

505 62. S. Elbaum-Garfinkle, Y. Kim, K. Szczepaniak, C.C.-H. Chen, C.R. Eckmann, S. Myong, et al., The
506 disordered P granule protein LAF-1 drives phase separation into droplets with tunable viscosity and
507 dynamics. *Proc Natl Acad Sci*. **112**, 7189–7194 (2015).

508 63. M. Feric, N. Vaidya, T.S. Harmon, D.M. Mitrea, L. Zhu, T.M. Richardson, et al., Coexisting Liquid
509 Phases Underlie Nucleolar Subcompartments. *Cell*. **165**, 1686–1697 (2016).

510 64. D.M. Mitrea, J.A. Cika, C.B. Stanley, A. Nourse, P.L. Onuchic, P.R. Banerjee, et al., Self-interaction
511 of NPM1 modulates multiple mechanisms of liquid-liquid phase separation. *Nat Commun*. **9**, 1–13
512 (2018).

513 65. M. Okuwaki, M. Tsujimoto, K. Nagata, The RNA Binding Activity of a Ribosome Biogenesis Factor,
514 Nucleophosmin/B23, Is Modulated by Phosphorylation with a Cell Cycle-dependent Kinase and by
515 Association with Its Subtype. *Mol Biol Cell*. **13**, 2016–2030 (2002).

516 66. S.S. Negi, M.O.J. Olson, Effects of interphase and mitotic phosphorylation on the mobility and
517 location of nucleolar protein B23. *J Cell Sci*. **119**, 3676–3685 (2006).

518 67. A.A. Van Hooser, P. Yuh, R. Heald, The perichromosomal layer. *Chromosoma*. **114**, 377–388 (2005).

519 68. Y. Hayashi, K. Kato, K. Kimura, The hierarchical structure of the perichromosomal layer comprises
520 Ki67, ribosomal RNAs, and nucleolar proteins. *Biochem Biophys Res Commun*. **493**, 1043–1049
521 (2017).

522 69. C. Wurzenberger, D.W. Gerlich, Phosphatases: Providing safe passage through mitotic exit. *Nat Rev*
523 *Mol Cell Biol*. **12**, 469–482 (2011).
524 70. L.A. Pinna, A. Donella-Deana, Phosphorylated synthetic peptides as tools for studying protein
525 phosphatases. *BBA - Mol Cell Res*. **1222**, 415–431 (1994).
526 71. Z. Dai, N.G. Dulyaninova, S. Kumar, A.R. Bresnick, D.S. Lawrence, Visual Snapshots of Intracellular
527 Kinase Activity at the Onset of Mitosis. *Chem Biol*. **14**, 1254–1260 (2007).
528 72. S. Martini, T. Soliman, G. Gobbi, P. Mirandola, C. Carubbi, E. Masselli, et al., PKCε Controls Mitotic
529 Progression by Regulating Centrosome Migration and Mitotic Spindle Assembly. *Mol Cancer Res*. 3–
530 16 (2017).
531 73. N. Brownlow, T. Pike, D. Zicha, L. Collinson, P.J. Parker, Mitotic catenation is monitored and
532 resolved by a PKC-regulated pathway. *Nat Commun*. **5**, 1–13 (2014).
533 74. D.G. Hardie, AMP-activated/SNF1 protein kinases: Conserved guardians of cellular energy. *Nat Rev*
534 *Mol Cell Biol*. **8**, 774–785 (2007).
535 75. M.R. Banko, J.J. Allen, B.E. Schaffer, E.W. Wilker, P.P. Tsou, J.L. White, et al., Chemical Genetic
536 Screen for AMPKα2 Substrates Uncovers a Network of Proteins Involved in Mitosis. *Mol Cell*. **44**,
537 878–892 (2011).
538 76. D.M. Gwinn, D.B. Shackelford, D.F. Egan, M.M. Mihaylova, A. Mery, D.S. Vasquez, et al., AMPK
539 Phosphorylation of Raptor Mediates a Metabolic Checkpoint. *Mol Cell*. **30**, 214–226 (2008).
540

541

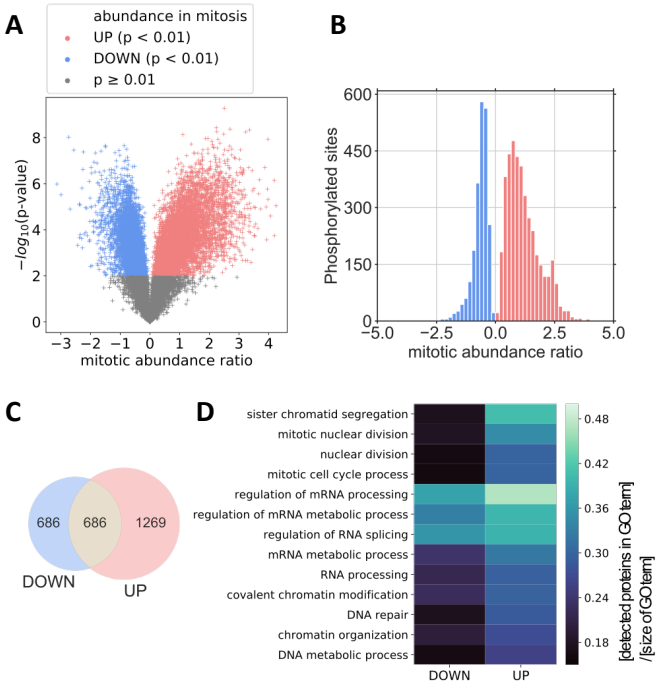

Yamazaki et al. Figure 1

542

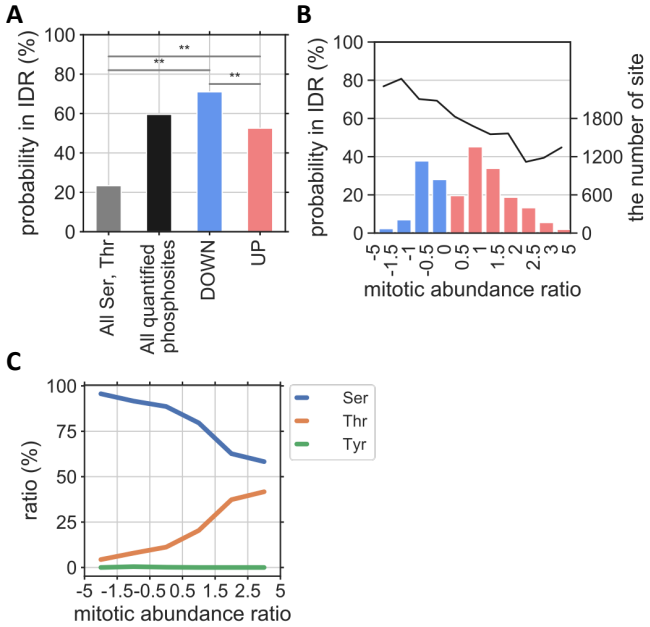

Yamazaki et al. Figure 2

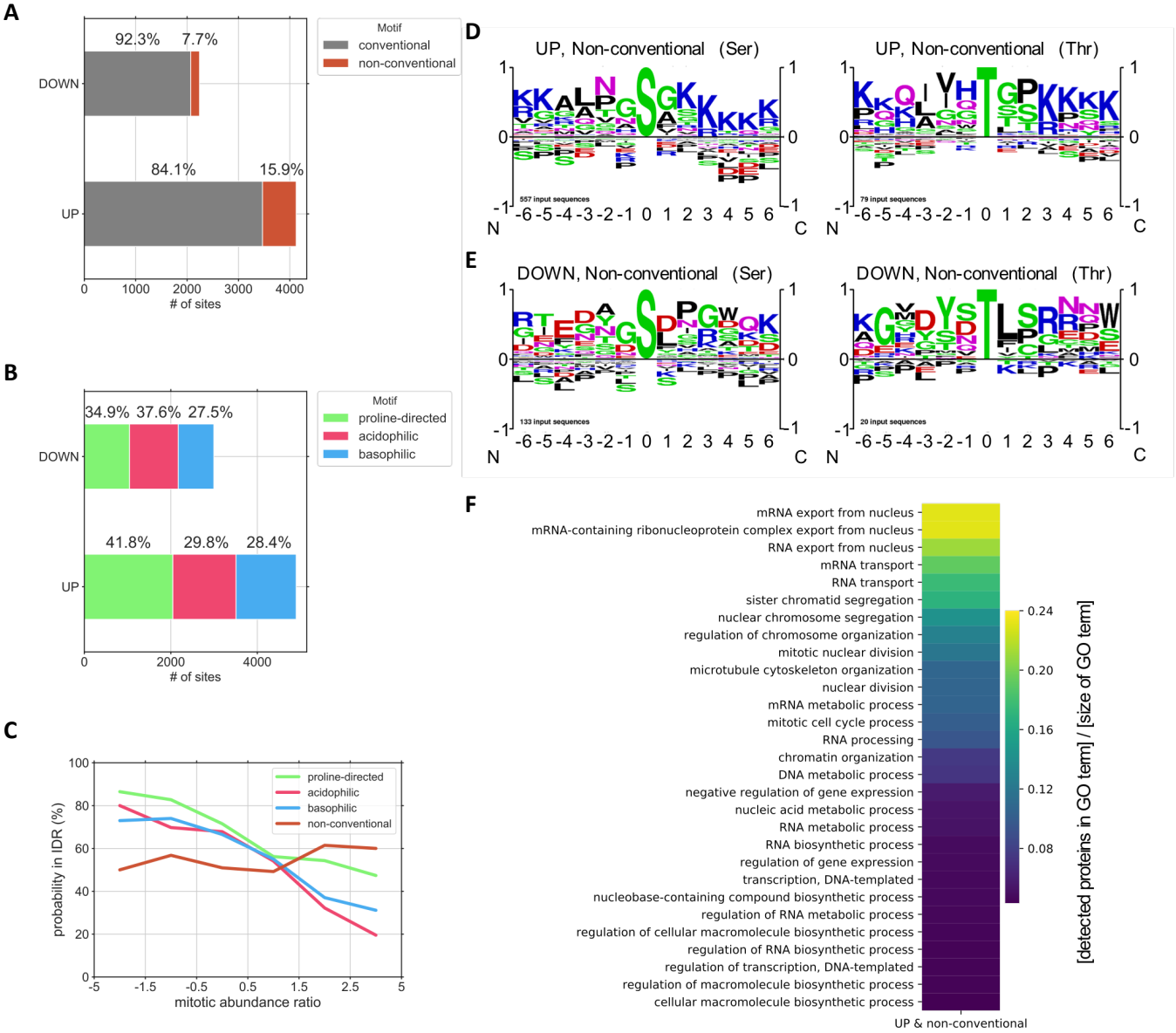

Yamazaki et al. Figure 3

544 # Figure Legends

545

546 **Figure 1.**

547 Quantification of mitotic phosphorylation by tandem mass tag analysis and gene ontology analysis on detected
548 proteins. (A) Volcano plot of the TMT-analysis. The p-values and abundance ratios of individual
549 phosphopeptides were plotted. Peptides with a $-\log_{10}$(p-value) <2 (grey) were eliminated from the subsequent
550 analyses. Positive (red) and negative (blue) peptides were extracted and subjected to subsequent analyses. (B)
551 Histogram of the abundance ratio. UP (red) and DOWN (blue) sites are distinguished. (C) Venn diagram of
552 the number of proteins containing UP and/or DOWN sites. (D) Gene ontology analysis of phosphoproteins
553 containing UP or DOWN sites. Biological process terms were obtained using DAVID. The number of
554 proteins identified in this study was divided by the total number of proteins associated with each term. Shown
555 are several terms relatively abundant for peptides with UP and DOWN sites.

556

557 **Figure 2.**

558 Structural properties and modified residues of mitotic phosphosites. (A) Probability of phosphosites existing
559 in intrinsically disordered regions. The IDR probabilities of all Ser and Thr residues, phosphosites, UP sites,
560 and DOWN sites are plotted. $^{**}P < 0.01$. (B) Relationship between IDR probability and abundance ratio. (C)
561 Relationship between phosphosite amino acid residue and abundance ratio.

562

563 **Figure 3.**

564 Neighboring sequences of mitotic phosphosites and the detected mitotic unconventional phosphorylation
565 motif. (A, B) Ratio of conventional and non-conventional motifs (A) and ratio of individual conventional
566 motifs (B) in UP and DOWN sites. (C) Relationship between IDR probability and abundance ratio for

567 individual conventional and non-conventional motifs. (D, E) Logo analysis of residues flanking UP (D) and
568 DOWN (E) sites in non-conventional motifs. Results for phospho-serine (left) and phospho-threonine (right)
569 are shown. (F) Gene ontology (biological process) analysis of proteins with UP sites in non-conventional
570 motifs. The number of proteins identified was divided by the total number of proteins associated with each
571 term.

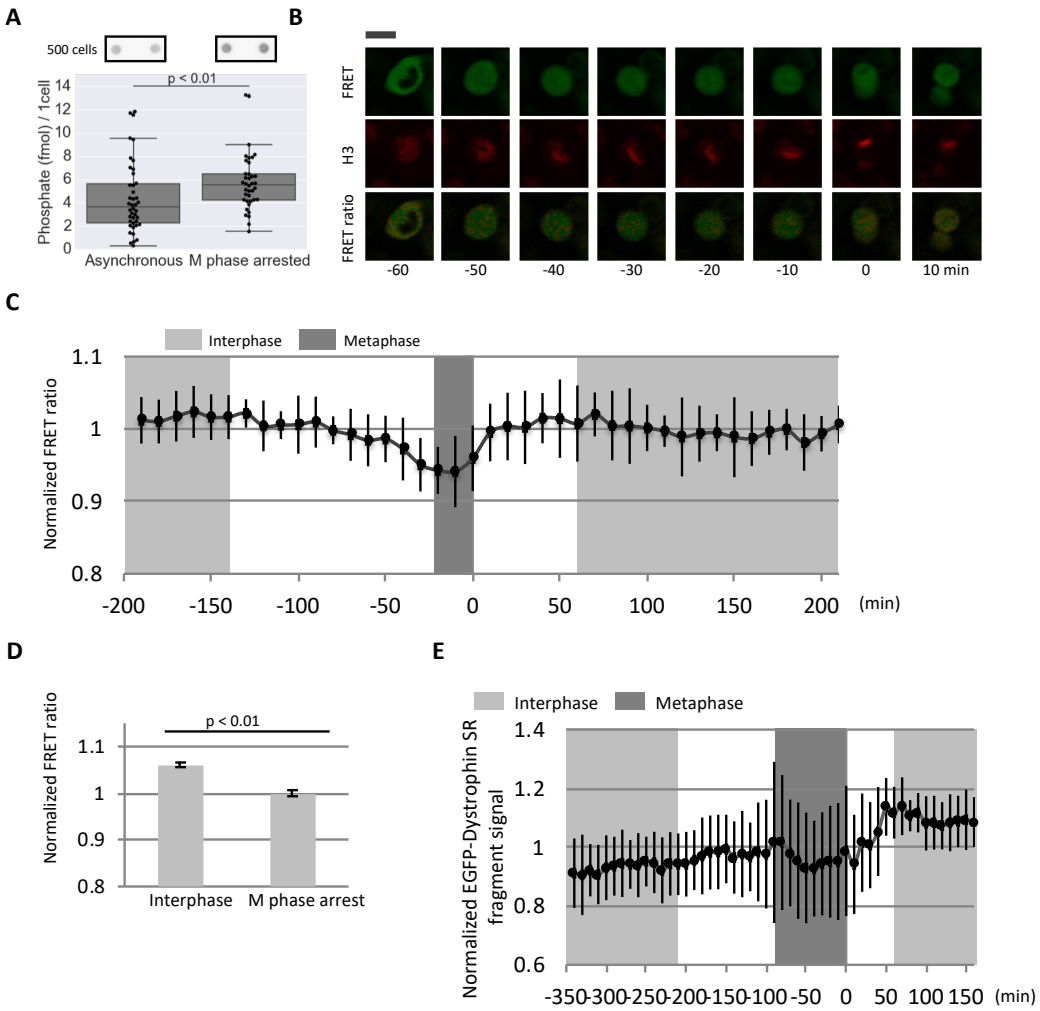

Yamazaki et al. Figure S1

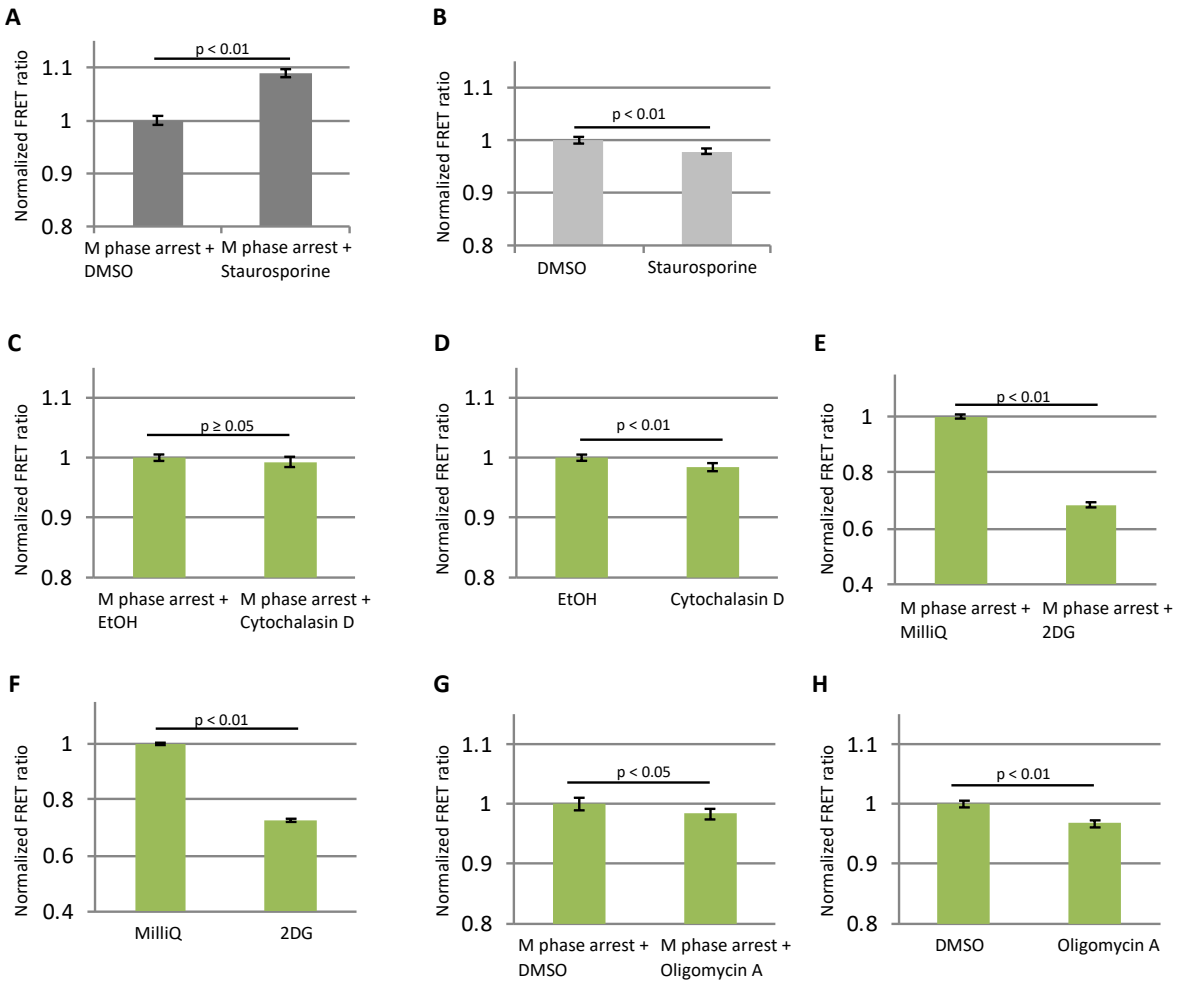

Yamazaki et al. Figure S2

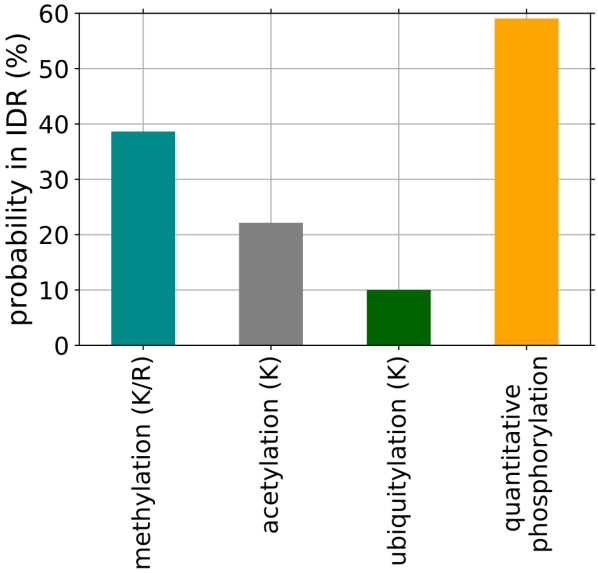

Yamazaki et al. Figure S3

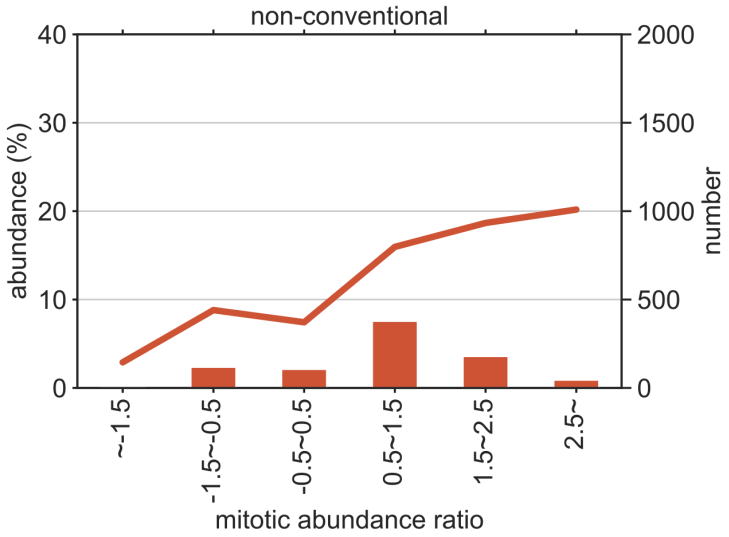

Yamazaki et al. Figure S4

576 ## Supplemental Figure, Table and Legends

577 **Figure S1.**

578 Total phosphoprotein amount increases and intracellular ATP level decreases during mitosis. (A) The amount
579 of phosphate on proteins in asynchronous and nocodazole-treated HeLa cells was quantified using pIMAGO
580 and streptavidin HRP conjugate. Dot-blot analysis of the lysate of ~500 cells is shown. The data points were
581 obtained from three independent experiments, and outliers were eliminated in each experiment based on the
582 inter-quartile range. Significance was assessed using the Mann–Whitney *U*-test. (B, C) Quantification of the
583 cytoplasmic ATP level during mitosis. HeLa cells expressing ATeam and mPlum-histone H3 were observed
584 by live-cell time-lapse imaging. Representative fluorescence images of FRET signal, mPlum signal, and
585 acceptor/donner ratio are shown. Scale bar: 20 μm (B). Time 0 was defined as the time chromosomes began to
586 segregate at anaphase onset. The acceptor/donner ratio was quantified in images, normalized to that of cells in
587 interphase, and plotted versus time (C). Data were collected from 16 cells, and each data points corresponds to
588 at least 8 cells. Error bars represents S.D. (D) Comparison of cytoplasmic ATP level between non-treated and
589 nocodazole-treated HeLa cells. HeLa cells expressing ATeam were treated with 2 mM thymidine for 18 h and
590 released to DMEM with 10% FBS for 1 h. The cells were then treated with or without 0.2 μM nocodazole for
591 10 h and observed by confocal fluorescence microscopy. The acceptor/donner ratio was quantified in the
592 obtained images and summarized. Data were collected from more than 100 cells. Values were normalized to
593 those of nocodazole-treated cells. A reduction in signal in mitosis was observed, as was the case in living cells
594 shown in B and C. Error bars represent 95% CI. Significance was assessed using Welch's *t*-test. (E) The
595 experiment described in Figure S1B and C was performed with EGFP-tagged dystrophin. Data were collected
596 from 13 cells, and each data point corresponds to at least 7 cells. Error bars represent S.D.

597

598 **Figure S2.**

599 Protein phosphorylation decreases the intracellular ATP level during mitosis. The experiment described in
600 Figure S1D was performed in the presence of various inhibitors in M-phase–arrested cells (A, C, E, G) and
601 non-synchronized cells (B, D, F, H). For M-phase arrest, HeLa cells were treated with thymidine for 18 h, and
602 after incubation with normal medium for 1 h, the cells were treated with 0.2 μM nocodazole for 10 h. (A, B)
603 Cells were treated with 1 μM staurosporine, a universal inhibitor of kinases for 1 h. (C, D) Cell were treated
604 with 1 μM cytochalasin D, an inhibitor of actin polymerization, for 1 h. (E, F) Cells were treated with 10 mM
605 2-deoxy-D-glucose (2DG), an inhibitor of glycolysis, for 1 h. (G, H) Cells were treated with 12.6 μM
606 oligomycin A, an inhibitor of oxidative phosphorylation, for 1 h. The acceptor/donner ratio was quantified in
607 the obtained images and normalized to that in the absence of the inhibitor. Error bars represent 95% CI.
608 Significance was assessed using Welch's *t*-test.
609
610 **Figure S3.**
611 Probability of post-translational modifications occurred in IDR. Amino acid residues and its flanking amino
612 acid sequences for methylation (15,283 sites), acetylation (20,875 sites) and ubiquitylation (96,796 sites) were
613 extracted from PhosphositePlus, and were subjected to the analysis of IDR as described in Figure 2. As a
614 comparison, the result of phosphosites obtained in this study is also plotted.
615
616 **Figure S4.**
617 Phosphosites at non-conventional motif. The number of phosphosites at non-conventional motif (right axis)
618 and its percentage (left axis) was plotted against mitotic abundance ratio.
619
620 **Table S1. Dataset from mass-spec analyses**
621

622

623 **Table S2. A list of proteins which carries NBC motifs and are known to be phosphorylated by AMPK.**

624